The Meteoritical Society

Meteoritics & Planetary Science 44, Nr 7, 1033–1049 (2009)
Abstract available online at http://meteoritics.org

The use of Auger spectroscopy for the in situ elemental characterization of sub-micrometer presolar grains

Frank J. STADERMANN[1*], Christine FLOSS[1], Maitrayee BOSE[1], and A. Scott LEA[2]

[1]Laboratory for Space Sciences, Physics Department, Washington University, CB 1105,
1 Brookings Drive, St. Louis, Missouri 63130, USA
[2]Pacific Northwest National Laboratory, Richland, Washington 99352, USA
[*]Corresponding author. E-mail: fjs@wuphys.wustl.edu

(Received 03 October 2008; revision accepted 19 May 2009)

Abstract—Presolar grains are small samples of stardust that can be found at low abundances in some of the most unaltered types of extraterrestrial materials. While earlier laboratory studies of stardust mainly focused on grain types that can be extracted from bulk meteorites by acid dissolution techniques, such as silicon carbide and graphite, recent analyses of presolar silicates rely on isotope imaging searches for locating these grains in situ. Since presolar silicates are generally less than a micrometer in diameter and represent at best only a few hundred ppm of their host materials (e.g., primitive meteorites or interplanetary dust particles), locating and studying these particles can be analytically challenging. Recently, we began using scanning Auger spectroscopy for the in situ elemental characterization of presolar silicate grains as a complement to NanoSIMS isotopic studies for obtaining spatially matched compositional data. Auger spectroscopy is a well-established analytical technique for elemental characterizations in the material sciences, but has not been widely used in geological applications. We discuss the application of this technique to sub-micrometer sized silicate grains and address practical issues such as sample preparation, measurement settings, spatial resolution, data processing, and elemental quantification.

INTRODUCTION

Many types of extraterrestrial materials, such as meteorites, micrometeorites, interplanetary dust particles (IDPs), lunar and cometary samples, are being studied in the laboratory with continually improving analytical resolution and sensitivity in an effort to learn about the processes that led to their formation and about their histories in different environments throughout their lifetimes. A ppm-level component of some of these samples are sub-micrometer to micrometer sized presolar grains which were first discovered during the search for the carrier phases of isotopically anomalous noble gas components in meteorites (Lewis et al. 1987; Tang and Anders 1988). These inclusions are characterized by extremely anomalous isotopic compositions which identify them as stellar condensates that predate their host materials and the solar system (e.g., Bernatowicz and Walker 1997; Zinner 2007). Detailed studies of the isotopic and mineralogical compositions of such presolar grains and comparisons with stellar evolution and grain formation models can provide important clues about nucleosynthesis and galactic chemical evolution (Meyer and Zinner 2006), as well as about grain survival in the interstellar medium and in different solar system reservoirs (Huss 1997, 2004). Any laboratory measurement of presolar grains is analytically challenging due to the small size of these objects, but the study of carbonaceous (e.g., silicon carbide, graphite, diamond) and oxide (e.g., corundum, spinel) presolar grains is somewhat facilitated by the fact that these species can be concentrated by extraction from bulk meteorites through series of chemical dissolution and physical separations (Amari et al. 1994).

Although high abundances of interstellar and circumstellar dust grains with silicate compositions can be observed astronomically (Molster and Waters 2003), such grains were long absent from the inventory available for laboratory research (Zinner 1997). Unlike other grain types, presolar silicates cannot be extracted from bulk meteorites through chemical dissolution because of the overwhelming abundance of silicates with a solar system origin. Instead, these grains have to be located by isotope imaging searches in situ and presolar silicates were discovered in IDPs and primitive meteorites after such searches became analytically feasible (Messenger et al. 2003; Nguyen and Zinner 2004;

Nagashima et al. 2004). Presolar silicates can be identified on the basis of their anomalous O isotopic composition (Messenger et al. 2003; Nguyen and Zinner 2004; Nagashima et al. 2004), and a particularly useful tool for such isotope searches is represented by the Cameca NanoSIMS (SIMS = secondary ion mass spectrometry), an instrument that was specifically designed for high spatial resolution and high sensitivity studies (Slodzian et al. 1987; Hillion et al. 1993). In a typical setup, the 100 nm Cs^+ primary beam of the NanoSIMS is rastered over sample areas of 10×10 μm^2 to 20 $\times$ 20 μm^2, while simultaneously collecting secondary ions of $^{16}O^-$, $^{17}O^-$, and $^{18}O^-$, in addition to other species of interest. By determining the isotopic ratios in the acquired images, it is possible to identify regions whose isotopic compositions are significantly different from that of the (isotopically normal) bulk of the imaged area (Fig. 1). Using this approach, O-anomalous presolar grains were identified in IDPs (Messenger et al. 2003; Floss et al. 2006; Stadermann et al. 2006b), primitive meteorites (Nguyen and Zinner 2004; Mostefaoui and Hoppe 2004; Messenger et al. 2005; Nguyen et al. 2007; Bland et al. 2007; Floss et al. 2008; Floss and Stadermann 2009a; Vollmer et al. 2009), Antarctic micrometeorites (Yada et al. 2008), and Wild 2 cometary samples (McKeegan et al. 2006; Stadermann et al. 2008; Stadermann and Floss 2008a). Among the O-anomalous presolar grains discovered in these studies are not only silicates, but also various types of oxide species. Knowing only the O isotopic composition of a presolar grain already provides important clues about its possible stellar origin (Nittler et al. 1997), but additional elemental or mineralogical information is crucial for a comparison with astronomical data (Henning 2009). In many cases, the NanoSIMS isotopic measurement itself does not provide much additional information about the makeup of these presolar grains (see below) and a discovery, such as shown in Fig. 1, will only be the *first* step of a more comprehensive analysis chain. In this paper, we discuss analytical techniques that can be used as a complement to the NanoSIMS for the elemental characterization of sub-micrometer presolar grains.

Analytical Alternatives

We have identified Auger spectroscopy as a useful tool for the study of presolar grains and the main focus of this paper will be a detailed description of this technique. However, when faced with the analytical challenge of identifying microscopic presolar phases in situ, as outlined above, there are other approaches that can also be employed. Here we first discuss several of these alternative techniques that have successfully been used in the past.

NanoSIMS for Elemental Characterization

This is possibly the most straightforward approach to getting elemental information about presolar grains. Since the NanoSIMS can measure several (5 or 7, depending on the model) masses simultaneously, it is possible to obtain some elemental information in addition to isotopic ratios during the same measurements. A search for O isotopic anomalies, for example, could be accompanied by the detection of Si and MgO secondary ions with a detector setup of $^{16}O^-$, $^{17}O^-$, $^{18}O^-$, $^{28}Si^-$, and $^{24}Mg^{16}O^-$ while using a Cs^+ primary beam. The advantage of such an approach is that the elemental information is acquired from exactly the same analysis volume, that no additional measurement time is required, and that data are obtained even when the presolar grain sputters away during the SIMS measurement. The downside of this approach is that not all elements are easily measured in a given secondary ion polarity (hence MgO^- instead of Mg^- in the above example) and that certain assumptions have to be made about "likely" presolar grain compositions at the onset of a measurement. For example, it is improbable that such an analytical approach would have led to the successful identification of FeO as a new presolar phase (Floss et al. 2008). In addition, elemental identifications can be problematic when a grain comes close in size to the spatial resolution of the technique. Following the isotopic identification of a presolar grain with a separate second measurement in the NanoSIMS for the sole purpose of obtaining elemental information may be possible, but this would result in undesirable sample consumption.

Electron X-Ray Techniques for Elemental Characterization

A well-established analytical approach for elemental measurements in geological samples is electron beam X-ray analysis, either in scanning electron microscopy with energy-dispersive X-ray detection (SEM-EDX) or electron probe microanalysis with wavelength dispersive X-ray spectroscopy (WDS). Very high spatial resolutions of only a few nm can be achieved in secondary electron imaging, especially with the use of field emission electron sources. The spatial resolution of the X-ray elemental information, however, is primarily limited not by the electron beam diameter, but by the size of the X-ray excitation volume (Fig. 2), which is on the order of 1 μm under standard operating conditions (Goldstein et al. 1992). The spatial resolution can be improved by using lower primary beam energies, but this is complicated by the fact that the X-ray production region is also element- (and X-ray line-) dependent. Elemental characterization of presolar grains by electron X-ray techniques may be possible in certain cases (e.g., Mostefaoui and Hoppe 2004; Nguyen and Zinner 2004; Stadermann et al. 2006b), but it is difficult to avoid contributions from neighboring phases in the EDX analysis of grains smaller than ~500 nm.

TOF-SIMS for Elemental Characterization

In time-of-flight (TOF) SIMS all masses of secondary ions of a given polarity are measured simultaneously and this

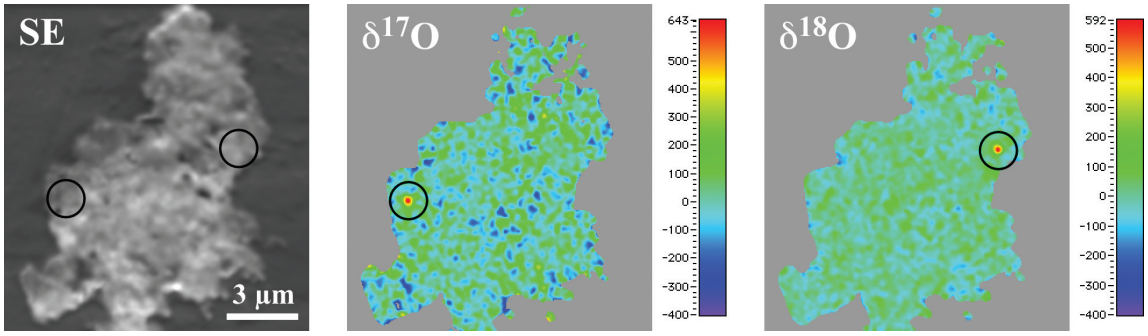

Fig. 1. Presolar grains in an IDP. In this NanoSIMS raster imaging measurement, secondary electrons (left) were detected along with the oxygen isotopes in a sample that has been pressed into high purity gold foil. The images of ^{16}O, ^{17}O and ^{18}O were processed to produce false color delta images. In delta notation, isotopic compositions are given as deviations from the normal isotopic ratios, in permil. Areas in blue-green are isotopically normal (i.e., $\delta^{17}O$, $\delta^{18}O \approx 0‰$) and two isotopically anomalous grains are visible in the circles. The presolar grains are about ~250 nm in diameter.

technique is therefore well suited for the identification of samples with completely unknown compositions (Stephan 2001). Since NanoSIMS and TOF-SIMS are related techniques, sample mounting requirements are similar, which makes it straightforward to perform complementary measurements on the same analysis areas (Stephan et al. 2003; Stadermann et al. 2005b; Bland et al. 2007). Although TOF-SIMS measurements can have a spatial resolution of 200 nm under ideal conditions (Stephan 2001), in general we found this to be insufficient for the elemental characterization of small presolar grains that are densely surrounded by other materials. Another issue with the combination of NanoSIMS and TOF-SIMS are the different apparent viewing and illumination angles of the two techniques (Fig. 3). Because the primary and secondary ion beams in the NanoSIMS are coaxial near the sample, images from the NanoSIMS appear as if the viewer looks straight down on a fully illuminated sample. This is not the case in TOF-SIMS where the primary ion beam is at an angle to the sample; surface topography can result in partial shading and distortion of the imaged features on the sample surface (Leitner et al. 2008). Such distorted images are difficult to align with the corresponding NanoSIMS images, particularly when the grains of interest are so small that a precise overlay of isotopic and elemental images is required.

TEM of Ultramicrotome Sections for Elemental Characterization

Transmission electron microscopy (TEM) clearly is the method of choice for elemental and structural measurements at a nanometer scale. We have demonstrated that NanoSIMS measurements can be performed directly in TEM ultramicrotome sections (Stadermann et al. 2005a), allowing spatially correlated isotopic and elemental/structural measurements on the same samples. This analytical combination is well suited for situations where NanoSIMS isotopic measurements are needed to complement a TEM study (Daulton et al. 2002, 2003, 2006; Croat et al. 2003, 2005; Stadermann et al. 2005a; Nakamura-Messenger et al. 2006; Matrajt et al. 2008) and works best when the TEM measurements precede the destructive SIMS sputtering. It is also possible to obtain spatially correlated TEM and NanoSIMS data by analyzing corresponding areas of *adjacent* ultramicrotome slices with respective techniques.

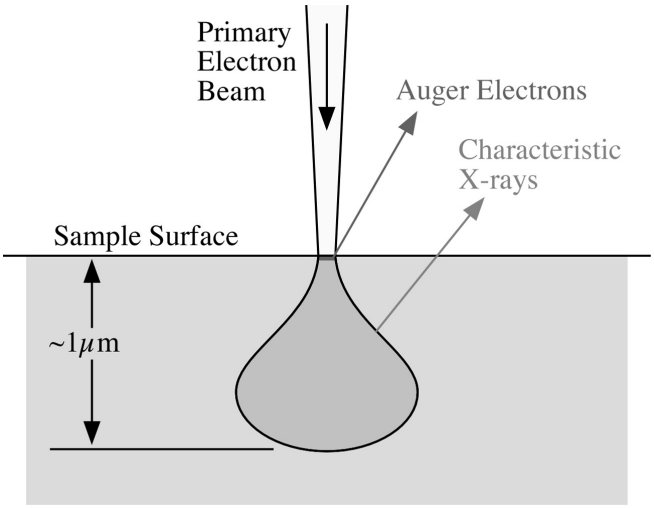

Fig. 2. Comparison of sample volumes analyzed by SEM-EDX and Auger spectroscopy. The characteristic X-rays that are used in EDX analyses originate from a large volume below the electron beam. Auger electrons are only detected from the uppermost few nanometers directly under the primary electron beam.

TEM of FIB Cutout Sections for Elemental Characterization

When NanoSIMS isotopic measurements are performed in sample types that are not directly accessible to TEM analyses, such as polished meteorite sections or particles pressed into a Au substrate, suitable electron-beam-transparent sections can be prepared afterwards. In many cases this can be accomplished with the focused ion beam (FIB) cutout technique, where a cross sectional vertical slice is cut from the material of interest (Stroud et al. 2004; Zega et al.

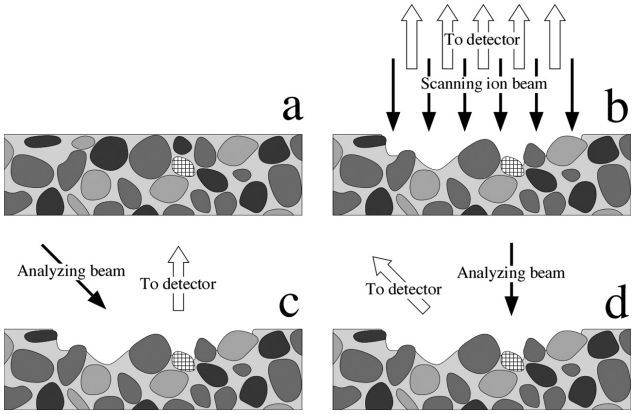

Fig. 3. Schematic of sample erosion and shading effects. An originally flat sample (a) consisting of a heterogeneous mix of sub-micrometer crystals in a fine-grained matrix develops significant topographic variations (b) during the NanoSIMS measurement due to varying sputter (beam erosion) rates in different minerals. An analytical system without coaxial beams (e.g., TOF-SIMS) will not be able to see the same surface that was analyzed by the NanoSIMS (e.g., the grain with the crosshatch pattern) due to shading. Note that for shading to occur it is irrelevant whether the primary (c) or the secondary (d) beam is at a non-normal angle.

2007; Graham et al. 2008). Such sections can then be used for TEM structural analyses of a part of the same sample that was previously analyzed with the NanoSIMS (e.g., Floss et al. 2004, 2006). In many regards, the combination of isotopic measurements and FIB-TEM studies overcomes most of the shortcomings of the other approaches discussed above and it allows TEM efforts to be focused on individual grains of interest. For many samples, this is the only way to obtain detailed structural information about individual grains. However, since the FIB-TEM approach is very labor-intensive, it is only suited for the analysis of a few particularly interesting grains. In addition, while the TEM analysis itself is practically non-destructive, the same is not true for the creation of a FIB cutout section which necessarily results in the removal of neighboring sample material. After the completion of the TEM measurements, the extracted section can be returned to the NanoSIMS for additional isotopic measurements (Floss et al. 2004; Stroud et al. 2009).

Although many of the described analytical approaches have their individual merits, we found that none of them represents a perfect match for the routine analysis of every presolar grain that has been found in situ with the NanoSIMS. Our search for a complementary analytical technique that allows non-destructive elemental measurements on the relevant scale of hundreds of nanometers directly in NanoSIMS-studied solid samples led us to Auger spectroscopy. We initially performed test measurements with the instruments at the National User Facility of the Environmental Molecular Sciences Laboratory (EMSL) of the Pacific Northwest National Laboratory (PNNL) in Richland, Washington, and at the Auger Demonstration Laboratory of Physical Electronics in Chanhassen, Minnesota (Stadermann et al. 2005c, 2006a). A new PHI 700 Scanning Auger Nanoprobe is now installed next to the NanoSIMS at Washington University. Below we describe technical aspects of the Auger technique and its application to the characterization of sub-micrometer presolar grains.

AUGER SPECTROSCOPY

The Auger effect was discovered independently by Pierre Auger and Lise Meitner in the 1920s and describes the emission of electrons with characteristic energies ("Auger electrons") from a sample that is irradiated with electrons in the 2–50 keV range (Auger 1975). The release of Auger electrons is a competing process to the emission of characteristic X-rays after a core hole is filled with an outer shell electron (Fig. 4). An Auger spectrometer is an instrument generally similar to an electron microprobe or SEM, except that it measures the kinetic energies of the emitted Auger electrons instead of X-ray energies, both of which carry information about sample composition. The fundamental difference between using X-rays and Auger electrons for elemental measurements is the size of the analytical volume, i.e., the region whose composition is probed. Characteristic X-rays are emitted from an onion shaped volume underneath the entry point of the electron beam and the size of this volume is in the 1 μm range under typical measurement conditions (Goldstein et al. 1992). Auger electrons with characteristic energies, on the other hand, originate only from the top few nanometers directly under the electron beam (Fig. 2). Deeper in the sample Auger electrons are produced as well, but these do not reach the surface with their original characteristic energy due to the short inelastic mean free path. The lateral resolution of elemental characterizations with Auger electrons is therefore tied foremost to the primary beam diameter. The achievable spatial resolution in Auger elemental raster imaging is in the tens of nanometers, which is more than sufficient for the characterization of presolar grains in the 100 nm size range. Since the Auger process requires a minimum of three orbital electrons, Auger spectroscopy can be used for all elements except hydrogen and helium. For a detailed discussion of the Auger technique see Thompson et al. (1985), Watts and Wolstenholme (2003), or Prutton and El Gomati (2006). Note that this analytical technique is referred to in the literature by a plethora of acronyms, such as AEES (Auger electron emission spectroscopy), AEM (Auger electron microscopy), AEMA (Auger electron microanalysis), AES (Auger electron spectroscopy), AS (Auger spectroscopy), EEAES (electron-excited Auger electron spectroscopy), EIAES (electron-induced Auger electron spectroscopy), EMAS (electron microprobe Auger spectroscopy), SAES (scanning Auger electron spectroscopy), and SAM (scanning Auger microscopy). A related technique, where X-ray photoemission is used to create electrons with characteristic kinetic energies is called XPS (X-ray photoelectron spectroscopy) or ESCA (electron spectroscopy for chemical analysis).

Auger spectroscopy is a well-established surface analytical technique in material science and the semiconductor industry (Watts and Wolstenholme 2003), but is only sporadically used for the analysis of geologic materials (e.g., Hochella et al. 1986a, 1986b). The latter is mainly due to problems with sample charging, which is a much bigger issue in Auger spectroscopy than in EDX analysis, since surface coatings obviously cannot be used in this surface analytical technique. While such problems may prevent a more widespread acceptance of Auger spectroscopy for geological analyses in general, we found that the characterization of sub-micrometer sized mineral grains represents an important niche application where favorable analytical conditions make this an exceptionally useful technique. Below we discuss the favorable parameters that aid in our use of the Auger spectrometer as a complement to the NanoSIMS.

Since the Auger spectrometer is essentially a scanning electron microscope, it shares many of the sample handling and mounting properties with this group of instruments. The NanoSIMS has much stricter sample size, vacuum compatibility, and surface flatness requirements, which ensures that practically any sample that can be analyzed in the NanoSIMS is also acceptable for the Auger spectrometer. One important advantage of using these two techniques for complementary isotopic and elemental sample characterization is due to the specific electron-optical design of the Auger spectrometers in this study. In these instruments the rotationally symmetrical "cylindrical mirror analyzer" (Kudo 2003) for the measurement of Auger electron energies is positioned around the primary electron beam column, resulting in coaxial incoming and outgoing (Auger) electron beam paths at the sample. This coaxial beam optics is fundamentally similar to the one used in the NanoSIMS (where primary and secondary ion beams are coaxial, Hillion et al. 1995) and ensures that both instruments "see" a sample from the same relative point of view, even on rough surfaces, without suffering from shadowing or uneven illumination by the primary beam. An important aspect of obtaining spatially correlated isotopic and elemental information from complementary NanoSIMS and Auger spectrometer measurements is precise alignment of the raster images from both instruments. Although both techniques, in theory, produce images of square raster areas, we find that some images show small rectangle or parallelogram distortions, which make it impossible to achieve perfect alignments by simply superimposing both images. However, with the use of image processing routines and the identification of fiduciary points in the images it is generally possible to attain overlays that are accurate down to the spatial resolution of the images.

While sample charging, as mentioned before, normally represents a severe complication in the Auger analysis of mineral grains, this issue is mitigated in many of the samples that we are interested in analyzing with the Auger instrument.

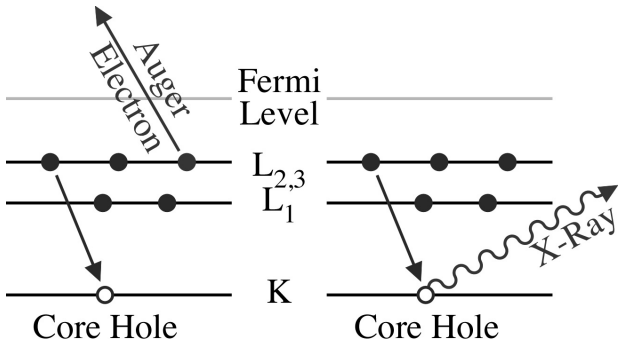

Fig. 4. Schematic of the Auger process: After the primary beam removes an inner shell electron, this vacancy can be filled with an electron from an outer shell. The resulting energy is released by the creation of either an Auger electron through an internal photoelectric process (left) or an X-ray photon (right), each with a characteristic energy.

There are a number of reasons that contribute to this favorable situation. Presolar silicate and oxide grains are generally only several hundred of nanometers in diameter, which is much less than the electron stopping range at a typical primary beam energy of 10 keV (Goldstein et al. 1992). This results in most of the electrical charge being deposited outside (below) the grain of interest. In the case of individual particles deposited on top of a conductive surface (e.g., Bose et al. 2007; Stadermann et al. 2007, 2008) the electrical charge is therefore immediately dissipated. This is also the case in the analysis of ultramicrotomed TEM sections on a conductive substrate (Meeker and Fleming 1986; Floss et al. 2007). Most of the other types of samples where we routinely find presolar grains, such as IDPs, Antarctic micrometeorites, and polished sections of the matrices of primitive meteorites, tend to be C-rich, with individual mineral grains embedded in a slightly conductive surrounding. Here, too, only a small fraction of the electrical charge is actually deposited inside the mineral grain being analyzed. Large polished sections of meteorites that are epoxy-mounted on a glass slide tend to charge as a whole under an electron beam without a proper conductive coating (typically C or Au) on the surface. Such coated samples are impossible to directly measure with Auger spectroscopy, which is only able to detect the coating material itself, but not the underlying sample of interest. However, the NanoSIMS isotope imaging measurement itself results in the (sputter) removal of the surface coating at precisely those locations that will be subsequently analyzed by Auger spectrometry. Thus, the sample area of interest is excavated, while the surrounding material is still covered with an electrically conductive coating (Fig. 5). In this situation, any charge buildup only needs to find a conductive path to the nearest remaining surface coating, which is less than 10 μm away from any point inside a 20 × 20 μm^2 raster area. Therefore, it is important when analyzing large non-conductive samples, such as thin sections, to keep narrow unsputtered (and thus conductive) areas between NanoSIMS

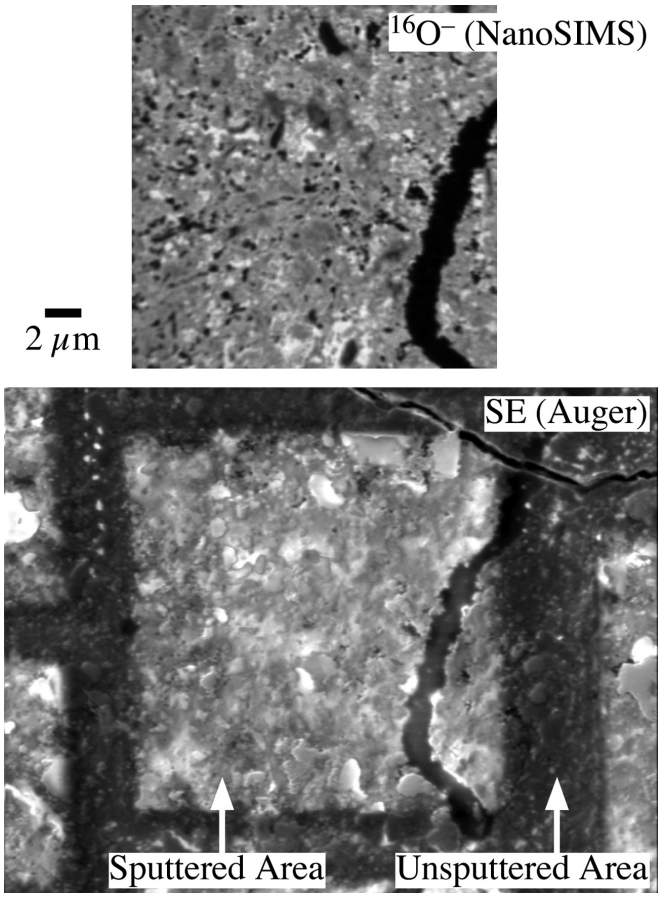

Fig. 5. Comparison of a $^{16}O^-$ NanoSIMS image and a secondary electron (SE) image of a polished section of ALHA77307 taken with the Auger Nanoprobe. Both images are shown at the same scale. The 20×20 μm^2 sputter area of the NanoSIMS is clearly visible in the SE image. The electrically conductive sample coating can still be seen between NanoSIMS raster areas. (Sample and NanoSIMS measurement from A. Nguyen).

analysis areas as shown in Fig. 5. We have found that many traditional methods to reduce sample charging in Auger spectroscopy, such as sample tilting or lowering the primary beam energy (Seah and Spencer 2000; Kelly 2003), are not required in the majority of our samples. Sample charging can easily be recognized in the Auger spectra, because characteristic peaks are typically shifted to higher kinetic energies (cf. discussion of Fig. 8 below).

Quantification

An Auger spectrum shows the count rates of detected secondary electrons as a function of their kinetic energy, from ~0 up to 3000 eV (Fig. 6). This distribution consists of Auger peaks with characteristic energies superimposed on a background of inelastically scattered primary and Auger electrons, as well as electrons from the secondary electron cascade (e.g., Seah et al. 1998). Since the Auger effect requires three different orbital electrons, groups of characteristic peaks are denoted by the names of the shells (K,

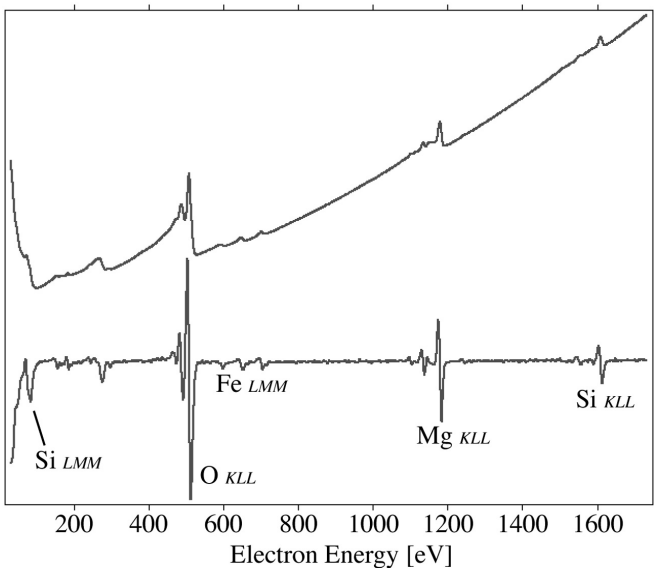

Fig. 6. Auger electron energy spectrum of a forsteritic olivine, taken with a 10 keV primary beam. The top curve is the direct spectrum and the bottom curve shows the same data in derivative form. The local maxima and minima of a given peak in the derivative spectrum can be used as starting points for a quantitative analysis. The small peak at 275 eV is due to C, a common surface contaminant.

L, M, N) of the electrons involved. The most common Auger emissions are of type KLL (cf. Fig. 4), LMM, and MNN. Qualitative elemental analysis alone may already be of value in many analytical situations; knowledge of which elements are present or absent at detectable levels in a given presolar grain, for example, can help distinguish between a silicate and an oxide grain (Floss and Stadermann 2009a). However, with the help of elemental sensitivity factors it is possible to go one step further in the interpretation of Auger electron spectra and extract relative quantitative information. One approach to Auger quantification involves determination of the areas under the peaks, after contributions from the broad backgrounds have been subtracted. Although this method is generally preferable in the case of simple Auger spectra (Seah 2003b), we found its application to be impractical for the mineral grains in our study, with varying elemental compositions and complex backgrounds. An alternative approach to quantification is based on the calculation of Savitzky-Golay smoothed and differentiated (Savitzky and Golay 1964) spectra as shown in Fig. 6. The peak-to-peak (maximum to minimum) heights in derivative Auger spectra ("Auger intensities") are then used together with element-specific sensitivity factors to determine elemental abundances in the analyzed sample. Since absolute secondary electron yields depend on a variety of external parameters, such as the primary electron current and the sample morphology, Auger quantifications are generally relative and normalized to 100% totals.

Auger elemental sensitivity factors depend on the specific Auger transition used for quantification as well as on

the primary beam energies and vary by more than two orders of magnitude. All commercial Auger instrument software comes with built-in sensitivity factor databases (e.g., Childs et al. 1995) for most of the periodic table and for common primary energies (such as 3, 5, and 10 keV). However, Auger sensitivity factors are also matrix-dependent (Seah 2003b) and while the database values work well for many applications in materials and semiconductor studies, we found that their direct application to silicate minerals would lead to large systematic errors for some elements. It became clear early on that any meaningful quantitative work on presolar silicates would require a systematic determination of new sensitivity factors on relevant mineral standards (see details below). We chose a primary beam energy of 10 keV as the standard value for most Auger studies, which results in an achievable spatial resolution (beam diameter) of ~20 nm. Although better spatial resolution can be obtained with higher primary electron energies, the value of 10 keV provides the best compromise (Ecke et al. 2007) between optimizing spatial resolution and reducing the Auger backscatter effect (see below).

For most of the rock forming elements the choice of which Auger transition to use for quantification is fairly straightforward. For some elements, however, we have to choose between an LMM peak below 100 eV and a KLL peak above 1000 eV (cf. Si in Fig. 6). Although the lower energy LMM peaks are frequently more sensitive, they appear in a more densely populated part of the spectrum with multiple overlaps and frequently a steep background. In addition, chemical shifts (see discussion further below) are more pronounced for the low energy transitions. All of these effects unnecessarily complicate the quantification efforts and we therefore decided to use the higher energy peaks whenever possible. Unless noted otherwise, the Auger peaks used in this study are O_{KLL} (510 eV), Mg_{KLL} (1188 eV), Al_{KLL} (1396 eV), Si_{KLL} (1621 eV), Ca_{LMM} (297 eV), and Fe_{LMM} (654 eV). The Fe peak used is the center one of the Fe_{LMM} triplet at 600, 654, and 705 eV.

Most of the Auger peaks that are relevant for this study are well separated from neighboring ones. Some samples also show Cs_{MNN} peaks (559 and 572 eV) due to earlier NanoSIMS measurements with a Cs^+ primary ion beam, but this contribution from implantation is minor and the peaks are well separated from the neighboring O and Fe peaks of interest. Some meteoritic sulfide and metal phases contain significant amounts of Ni in addition to Fe. By using the 654 eV Fe_{LMM} peak for quantification, it is possible to avoid overlaps with the strong Ni_{LMM} triplet at 718, 785, and 849 eV. A common surface contaminant is C and samples that have been raster imaged for extended periods of time in an SEM frequently develop surface coatings that are clearly visible as dark rectangles. These coatings are caused by the cracking of hydrocarbons under the electron beam and consist of a layer of C on the sample surface (Goldstein et al. 1992). Minor C contributions in the Auger spectra (e.g., Fig. 6) can be tolerated and do not significantly affect the relative intensities of the other peaks, but in some cases SEM-deposited C layers are so thick that C_{KLL} becomes the dominant peak in the Auger spectra. Thick layers of C will distort calculated elemental compositions, although it may be possible to correct for this effect in some cases (Smith 2005). The deposition of C may also occur under the electron beam of the Auger spectrometer itself, but this effect is highly sample- and vacuum-dependent. Non-outgassing samples can be raster-imaged for days in the Auger spectrometer without any significant C buildup when the analysis chamber pressure is in the 10^{-10} hPa range. The Auger spectrometer is equipped with an Ar sputter source that can be used for wide area cleaning of surface-contaminated samples. Although the sputter source is mounted to the side of the electron column, it is possible to achieve isotropic surface cleaning by rotating the sample during the Ar sputtering (Zalar 1985). In principle, this sputter cleaning may lead to the implantation of Ar in the sample surface, but we have not come across any samples that show a detectable Ar signal (the Ar_{LMM} peak would be at 219 eV).

Since we want to obtain compositional information from samples studied by SIMS, it is pertinent to evaluate the effects that ion sputtering might have on the sample properties to be determined with Auger spectroscopy. During SIMS measurements, a high energy, finely focused primary ion beam is rastered over the sample surface. Primary ions set off a collision cascade of sample atoms, which leads to a partial amorphization of the near-surface region of the sample and an ejection of both ionized and electrically neutral sample atoms and clusters into the vacuum. Because overall more material is ejected than primary ions are implanted, the SIMS measurement leads to a slow consumption of the sample. Despite the destructive nature of this analytical technique, sample consumption is actually minor in many applications. For example, under typical NanoSIMS isotope imaging conditions, less than 15% of a 200 nm olivine grain needs to be sputtered away in order to achieve a 10% precision of the $^{17}O/^{16}O$ ratio, which is sufficient to identify a presolar isotopic signature. A 5% precision can be achieved by consuming 50% of such a grain. It is therefore in most cases possible to perform Auger measurements on parts of the grains that were analyzed in the NanoSIMS, although obviously not on the same analysis volumes.

NanoSIMS O isotopic measurements are performed with a 16 keV Cs^+ primary beam, which hits the sample in normal direction. The range of the implanted Cs ions and thus the size of the affected sample region under these conditions is around 10–20 nm (Ziegler et al. 1985). The maximum lateral repositioning of surface atoms is in the same range and since this is below the intrinsic spatial resolution of the NanoSIMS, this mixing effect is negligible. It should be noted that extended sputtering does not lead to a continuously

broadening lateral mixing range, since lateral mixing and sample consumption are competing effects which rapidly reach an equilibrium value. Another potential consequence of sample sputtering is a change in the surface composition due to preferential sputtering. However, quantitative Auger elemental measurements in sputtered and unsputtered grains from the same silicate standard show that, within the current uncertainty (see below) of these measurements, there are no systematic changes in elemental compositions, except for the aforementioned addition of implanted Cs. We will revisit this issue once ongoing development efforts allow higher precision elemental quantifications of the Auger measurements.

While the ion bombardment of the sample turns out to be relatively benign with regard to subsequent Auger measurements, substantial alterations are observed as result of the interaction with the electron beam. Sample damage due to the electron beam is a well-known effect (e.g., Goldstein et al. 1992), which occurs in all electron beam instruments, including SEM, TEM and Auger spectrometer. Unfortunately, however, this type of sample damage affects the highly surface-sensitive Auger measurements more than other techniques. Electron beam effects are material-specific and while some samples can be analyzed with high intensity beams for extended periods of time in point analysis mode without any ill effects, other samples show alterations so rapidly that completely non-destructive measurements are nearly impossible (Pantano et al. 1998). The silicate grains that we are interested in studying fall into an intermediate range, where most damage can be reduced by a careful choice of analytical parameters. There is a wide array of possible types of electron beam damage, including structural changes and partial sample melting (Pantano et al. 1998), but not all damage types are equally important for our applications, particularly because some of the crystal structure has already been altered by the preceding ion beam bombardment of the mineral grains. We are mostly interested in those electron beam effects that can lead to changes in the sample's composition, which we want to determine with the Auger spectrometer. Such changes can result from adsorption onto the sample, desorption from the sample, or the redistribution within the sample (Baer et al. 2003). A detailed discussion of the mechanisms of such alterations is beyond the scope of this paper, but the net effect is a change of the sample's surface composition as a function of beam intensity and analysis time. We found the most practical approach to be a combination of reducing these electron beam effects by choosing appropriate measurement conditions and simultaneously monitoring the occurrence of possible compositional changes as much as possible. How this is accomplished is discussed below in some detail.

Electron beam damage is strongly correlated with the dose received and it is therefore critical to reduce both the beam current density at the sample surface and the analysis time as much as possible. As expected, we have seen the most dramatic changes in surface compositions in high-current stationary measurements with a finely focused beam. Simply reducing the primary beam current in the Auger spectrometer may not have the desired effect if it results in an increased analysis time. However, using a lower primary beam current has the advantage of slowing the development of compositional changes, so that their onset can more easily be determined, especially when a series of successive measurements is performed. We found it practical to reduce the beam current from a normal value of 10 nA to 0.25 nA, which still gives a sufficient secondary electron intensity for viewing the sample in raster imaging mode. Under these conditions, it is possible to acquire enough spectral information for a meaningful quantification in less than 30 minutes. To avoid electron beam damage as much as possible, it is important not to use a focused stationary beam, but to spread the beam over the entire grain of interest and thus reduce the current density. In theory, this could be done by defocusing the electron beam, but this is impractical in the case of submicrometer mineral grains, which cannot be easily located in a defocused raster image. However, it is possible to spread the beam over a larger surface region by measuring in raster mode. This has the advantage that the rectangular analysis region can easily be optimized for the grain's shape and size (Fig. 7). Since the electron beam is step-rastered over the analysis region during the measurement, it is important to choose a step size that is smaller than the beam diameter on the sample to avoid the creation of a grid pattern (e.g., Fig. 4 of Bentley et al. 2006). Another benefit of using a rastered beam instead of a stationary one is that measurements give averaged compositions, which is important for grains with internal heterogeneities.

Since electron beam damage or slight sample charging is unavoidable in some samples, it is crucial to carefully monitor the onset of compositional changes during measurements. This requires a deviation from the normal Auger spectrum acquisition mode, where data from sequential energy scans are continuously integrated for a single spectrum without any documentation of possible temporal changes. Instead, we acquire automated sequences of 10 to 20 shorter spectra of the same analysis area. Because of the low beam current and much shorter measurement time, an individual spectrum from such a measurement sequence is usually quite noisy and thus unsuitable for direct quantification (Fig. 8). However, potential changes in the larger peaks (including O) throughout the sequence, which may signal variations due to electron beam damage or charging, are generally quite noticeable. Another indication of beam damage that is frequently seen in silicate minerals is a shift of the Si peaks due to changes in the chemical structure (Hochella et al. 1986a). Although we use the Si_{KLL} peak for quantification, the chemical change from Si oxide to elemental Si is easier to observe at the larger Si_{LMM} peak,

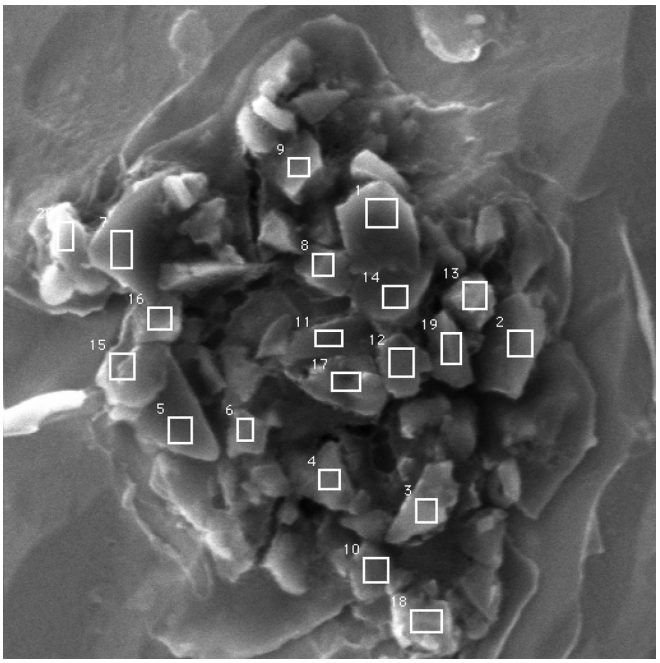

Fig. 7. Secondary electron image (10 µm × 10 µm) of dispersed standard grains on a gold substrate. The white boxes indicate the raster areas from which Auger electron energy spectra were acquired.

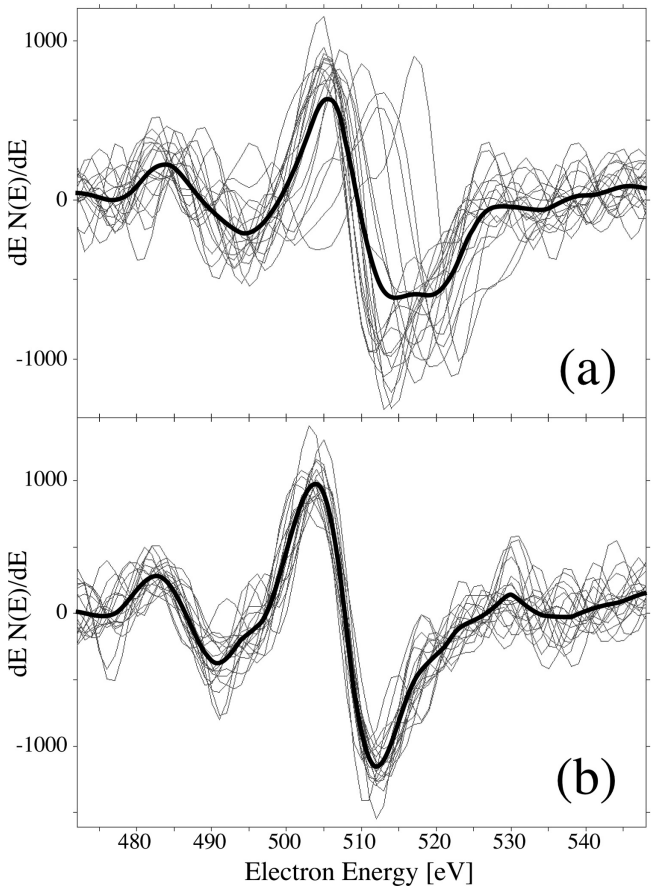

Fig. 8. Derivative Auger energy spectra of the O_{KLL} peak from the measurement of silicate standards. Individual spectra from a measurement sequence (gray) are in many cases too noisy for direct quantification and averaged spectra (black) are used instead. Acquiring sequences of many spectra on the same sample has the advantage that possible dynamic sample changes can be recognized. An obvious peak shift during measurement (a)—likely due to sample charging—signals that a quantitative interpretation will be difficult in this case. Since no shift is detected in measurement (b), a meaningful quantitative analysis can be based on the average of all spectra from this measurement sequence.

which can be seen to shift from 80 to 96 eV in some silicates during the course of an Auger measurement. The fact that Si oxide peaks are still observed in many silicates after they have been sputtered with the ion beam indicates that in such cases the long-range crystalline structure may be lost due to amorphization, yet most of the core structure is still intact at an atomic level. If no temporal change is seen in the spectra from a sample's measurement sequence, all data can be summed into a single spectrum which can then be used for quantification (Fig. 8). It is also possible to exclude some spectra from this summation if the onset of electron beam damage is noticed midway through the spectrum sequence. When damage cannot be avoided at all, it may be feasible to measure the rate of damage as a function of time and to extrapolate to zero time (Baer et al. 2003). Many silicate grains can be measured under the described analytical conditions without suffering extensive beam damage. As also observed elsewhere (Hochella et al. 1986b), we found this not to be the case for several carbonate minerals that we analyzed.

It is important to remember that the described damage occurs not only during Auger measurements, but during any exposure to electron beams. Care has to be taken not to damage the sample surface after the NanoSIMS measurement and before the Auger spectrum acquisition. Any sample documentation by high magnification SEM imaging should ideally be scheduled for after the Auger measurements. In some cases it may also be possible to shorten the Auger measurement itself (and thus the electron beam exposure) by foregoing the acquisition of a complete electron energy spectrum in favor of smaller energy windows of only the peaks of interest (Pantano et al. 1998), although this necessarily requires some prior knowledge of the sample's expected composition.

As mentioned earlier, it is not possible to obtain accurate quantitative results for silicate minerals with the sensitivity factors of the data processing software (Childs et al. 1995) which are optimized for material science and semiconductor applications. This is due to the matrix dependency of Auger sensitivity factors (Seah 2003b), but does not pose a major problem, as long as it is possible to obtain sets of reproducible sensitivity factors for the materials of interest. To test this approach, we have initially determined sensitivity factors for a range of silicate minerals with varying compositions as this has direct bearing on our studies of presolar silicates (e.g., Floss and Stadermann 2009a). Because of the aforementioned problems with sample charging and to be as close as possible

Table 1. Auger element sensitivity factors (at 10 kV).

Element	Auger transition	Energy (eV)	Sensitivity factor	Uncertainty (% rel.)
O	KLL	510	0.194	3.6
Mg	KLL	1188	0.234	9.4
Al	KLL	1396	0.160	24.9*
Si	KLL	1621	0.121	11.0
Ca	LMM	297	0.626	10.8
Fe	LMM	654	0.150	11.2

Uncertainties are given as relative percent values, e.g., a 10% relative uncertainty of a 30 at% value is ±3 at%.

*The large relative uncertainty for Al is due to the fact that the standards used only contain minor amounts of this element.

to actual silicate samples, we first focused on standards that were available in sub-micrometer grain sizes, such as pulverized silicates from Hofmeister and Pitman (2007). These standards include olivines with compositions ranging from Fo_{54} to Fo_{85}, as well as a variety of pyroxenes. Analyses followed the analytical protocols outlined above and consisted of measurements of at least 10 grains for each mineral type. The results from a few grains that were obvious contaminants were excluded from further processing. Sensitivity factors for six elements were then determined by least squares fitting of the Auger intensities to the nominal compositions of the standards. The atomic concentration × of any element a in a sample can be written as $X_a = N_a/\Sigma N_i = (I_a/S_a)/\Sigma (I_i/S_i)$, where N is the atom count per unit volume, I is the Auger intensity, and S is the sensitivity factor (Childs et al. 1995). A list of 10 keV sensitivity factors for our set of olivine and pyroxene standards is given in Table 1. All spectra were acquired in 1 eV steps and then processed with 7-point Savitzky-Golay smoothing/differentiation. The determined elemental sensitivity factors and their uncertainties are shown in Table 1. Figure 9 shows agreement between Auger and electron microprobe quantification results within a few percent for the olivine and pyroxene standards used, as well as for grains of SiO_2. We will continue to add other mineral types to the database, which will help extend the limited compositional range for some elements, and expand the sensitivity factor database to other relevant elements.

The uncertainty of the sensitivity factors given in Table 1 is the standard deviation of the Auger/electron probe ratios for the different elements in the mineral standards used. The actual uncertainty in the quantification of a single mineral grain also depends on individual measurement parameters that affect the "quality" of a given Auger electron energy spectrum. Factors that may degrade the precision of quantitative Auger measurements include sample charging, the presence of thick contamination layers, insufficient signal-to-noise ratios, and compositional changes due to electron beam damage. The latter two items are related to grain sizes and sizes of the Auger measurement areas. On larger grains, it is possible to raster the electron beam over larger areas, thereby reducing the beam current density. This

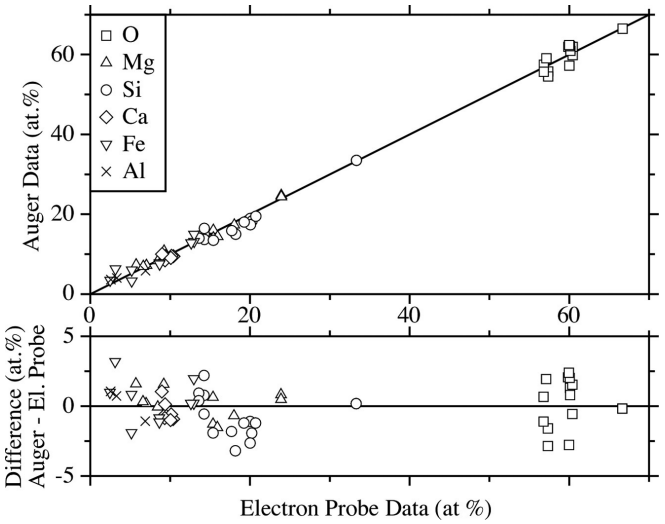

Fig. 9. Comparison of Auger and electron microprobe quantification data on silicate standards using silicate-specific sensitivity factors. Most points (each representing the average of multiple measurements on the same standard) fall close to the 1:1 correlation line (a). The deviations from the 1:1 line are shown magnified below (b). On a relative scale (deviation/abundance), the largest uncertainties are at the very low abundances, indicating the Auger peaks with the lowest signal to noise ratios. However, due to the fact that abundances are normalized to 100% totals, the uncertainties in low-abundance elements indirectly affect O data as well. The detection limits for Auger measurements in sub-micrometer silicate grains vary by element, but are generally in the few percent range. Only elements >2 at% were included in these quantifications.

in turn will allow for longer acquisition times while avoiding beam damage and the integration over such extended measurements will provide better signal-to-noise ratios. In other words, measurements of larger grains will generally give more precise quantitative results than those of smaller ones, as long as the grain sizes are not so large (several μm) that sample charging becomes the dominant issue. While the uncertainties of compositional Auger spectroscopic measurements on sub-micrometer silicates thus vary from case to case, the uncertainties given in Table 1 represent the current lower limits. We are testing different data processing models for the treatment of spectra with low signal-to-noise ratios, such as intensive peak broadening with a Gaussian function (Seah et al. 1998), and expect that this will help in reducing the uncertainties currently attached to the sensitivity factors. It should also be pointed out that some of the variations observed in the comparison between quantitative electron probe and Auger data may be due to the difficulty of obtaining standards whose homogeneity is guaranteed on the relevant scale of 100 nm. Once a mineral standard is pulverized to sub-micrometer fragments it becomes difficult to completely avoid contaminants either in the form of particles or as surface coatings on individual grains.

As mentioned earlier, detailed knowledge of elemental sensitivity factors is not required for simple tasks as

distinguishing silicate grains from oxides and qualitative measurements alone are in most cases sufficient for identifying Mg- versus Fe-rich silicate phases (cf. Fig. 11). To evaluate the practical usefulness of more challenging Auger quantifications in sub-500 nm grains, we have used data from 114 standard grains to test, for example, whether the measurements allow a distinction between olivine and pyroxene grains. A histogram of the [Fe+Mg(+Ca)]/Si ratio for these grains is shown in Fig. 10. For this ratio pyroxene, $(Mg,Fe,Ca)_2Si_2O_6$, has a nominal value of 1 and olivine, $(Mg,Fe)_2SiO_4$, of 2. The distributions for both mineral types show some deviations from the nominal values and are approximated by Gaussian normal distribution curves in the diagram. Although there is some overlap between the two curves, both populations are clearly distinguishable. This means that while it may not always be possible on an individual grain basis to unequivocally distinguish between an olivine- and a pyroxene-like composition, on a statistical basis predominately olivine-like grain populations will be markedly different from those that are dominated by pyroxene-like grains (Floss and Stadermann 2009a).

The best achievable detection limits in Auger spectroscopy at high spatial resolution are around 1 at.% (Ecke et al. 2007), but this value only applies to "ideal" samples where measurements are not restricted (in terms of beam current and analysis time) by the possibility of beam damage or sample charging. In our study of small silicate grains we found actual detection limits to be both element- and noise-level-dependent. To identify an elemental peak in the Auger spectrum, the peak has to be recognizable above the level of the random background noise (cf. Fig. 8). Elements with a higher sensitivity factor (Table 1) will have more pronounced peaks in the derivative Auger spectra than other elements with the same atomic abundance. For example, Al, measured as Al_{KLL}, has a detection limit that is higher (worse) than that of the very sensitive Ca_{LMM}. The noise level in an Auger spectrum can generally be reduced by increasing either the beam current or the analysis time, but, as discussed above, these options are not available in the microanalysis of silicate minerals due to the possibility of electron beam damage. With the signal-to-noise ratio typically obtained in the Auger analysis of sub-500 nm mineral grains, the practical detection limits for the elements shown in Table 1 are on the order of several at.%.

When analyzed with a low beam current density as described, we found the small mineral standard grains to be quite stable under the electron beam for typical analysis times. None of the analyzed olivine and pyroxene grains showed any visual changes in grain appearance when comparing before and after SE images and no significant compositional drifts were observed in the repeated Auger scans. The quantitative effects of electron beam damage are highly material-dependent (Baer et al. 2003), but there is little information about the mineral types (olivine, pyroxene) that are relevant in this study. However, empirical studies of

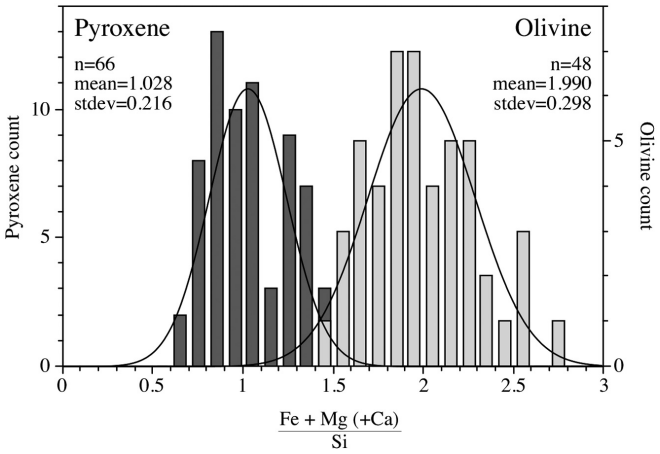

Fig. 10. Histogram of compositional variations in the quantitative Auger measurements of 66 pyroxene (dark) and 48 olivine (light) standard grains. Both groups show deviations from the nominal [Fe+Mg(+Ca)]/Si values of 1 for pyroxene and 2 for olivine, but the populations are clearly distinguishable.

amorphous SiO_2 surfaces indicate that compositional changes can be observed within minutes at beam current densities that are significantly lower than the ones typically used in our studies. That we do not generally see such temporal changes in our measurements of mineral standards may be due to one or more of the following reasons: (a) There may be a material-dependent difference between the SiO_2 films used and the ferromagnesian silicates in our study. (b) We are analyzing individual, sub-micrometer sized mineral grains and not polished sections of larger crystals. This dramatically alters the physical environment of the analyzed material with respect to sample charging, thermal conductivity, and electron beam energy deposition. (c) Although most beam effects are measured only as function of electron beam current density, there may also be a dependency on the absolute beam current (or analysis area). Beam damage effects that are due to sample heating, for example, may be less pronounced when only a small surface area is hit with the electron beam (at constant current density) and any heat buildup can easily dissipate into the surrounding area that is not heated by the electron beam.

Imaging

The Auger Nanoprobe can also be used for elemental distribution imaging at high spatial resolution. Measurement times depend on an element's Auger peak height and can take up to several hours for a single elemental raster image in 256 × 256 pixels. Since the images for all elements of interest have to be acquired sequentially, the total analysis time for multi-elemental maps can be exceedingly long, even with a 10 nA beam current. Auger elemental imaging can be done for all elements, with the exception of H and He, including elements that may be difficult to measure with other techniques such as N or the noble gases. In the case of N there is a particular advantage when compared to SIMS measurements, because Auger N imaging can show the spatial distribution of N

independent of C (Floss et al. 2007), unlike in SIMS, where N is typically measured as the CN^- cluster. Since the imaging mode does not acquire a full Auger electron energy spectrum of each pixel, the resulting data cannot directly be used for quantification. Nevertheless, the qualitative information from Auger elemental distribution maps can be very useful for identifying individual grains in heterogeneous surroundings, for determining grain shapes and sizes that are not obvious from the SE images, and to visualize the internal makeup of individual grains (Fig. 11). As is the case for spectrum acquisition, it may be beneficial to acquire sequences of images for each element, which can later be added for improved signal-to-noise ratio. Retaining sequential images has the advantage that any possible change in the sample (e.g., due to electron beam damage) can be directly identified.

The spatial resolution in Auger elemental measurements can be somewhat diminished due to the "backscatter effect" (Seah 2003a). Although most Auger electrons are created in the direct interaction between the primary electron beam and the sample, some can also be triggered by sideways scattered electrons in the area immediately surrounding the primary beam. The exact impact of the backscatter effect depends on the primary beam energy, the composition of the material directly under the electron beam, and the average composition of the directly surrounding material (Powell 2004). In practice, we found this effect to be of minor importance in most of our measurements, as is corroborated, e.g., by the presence of relatively sharp compositional boundaries in elemental maps, such as shown in Fig. 11. The Mg line profiles shown in panel (d) of this figure indicate an edge width of the Mg-rich presolar grain of ~40 nm, which represents a combination of the intrinsic spatial resolution of the Auger imaging and the sharpness of the phase boundary after Cs sputtering. In quantitative measurements the only situation where this backscatter effect leads to significant artifacts is in the analysis of very small grains that are completely void of an element which is highly abundant in all surrounding phases (Floss and Stadermann 2009b), such as a 100 nm, O-free SiC crystal within an O-rich silicate environment.

DISCUSSION

Although we have only recently begun to apply Auger spectroscopy to the study of presolar grains, there have been occasional studies that made use of this analytical technique in the wider field of cosmochemistry for more than 30 years. Many of the earlier investigations were done with Auger instruments that would have been insufficient for our current study in terms of spatial resolution and sensitivity, yet not all applications require a sub-micrometer resolution. The primary emphasis has previously been on studies of the effects of the space environment on the surface properties of lunar samples (Gold et al. 1974, 1976, 1977; Dran et al. 1977; Dikov et al. 1999). Other studies looked into the fracture behavior of Fe-Ni meteorites (Marcus and Hackett 1974), the surface chemistry of several stratospheric dust particles (Mackinnon and Mogk 1985; Mogk et al. 1985), and elemental properties of Murchison matrix material (Meeker 1986; Radicati di Brozolo et al. 1991). Overall, these applications have been rather sporadic, possibly due to the lack of a dedicated Auger instrument for use in cosmochemistry and the fact that multi-element imaging measurements can be very demanding with respect to instrument time.

We have found the use of Auger spectroscopy of NanoSIMS-studied samples particularly compelling because there are no viable analytical alternatives for the routine in situ elemental analysis of large numbers of presolar silicate and oxide grains on a sub-micrometer scale. We have developed the analytical protocols for quantitative elemental measurements, but even as a qualitative tool Auger spectroscopy can provide important information about elemental distributions, grain heterogeneities, and particle identification. To date we have used this technique for the elemental and chemical characterizations of NanoSIMS-identified phases in primitive meteorites (Marhas et al. 2006; Bose et al. 2007, 2008b; Floss and Stadermann 2007, 2008a, 2008b, 2009a, 2009b; Nguyen et al. 2007, 2008; Vollmer et al. 2007, 2008, 2009; Floss et al. 2008), IDPs (Floss et al. 2006, 2007), Antarctic micrometeorites (Yada et al. 2006, 2008), cometary samples (Stadermann et al. 2007; Stadermann and Floss 2008a), or a combination thereof (Floss et al. 2005; Stadermann et al. 2005c, 2006a; Bose et al. 2008a). The identification of circumstellar Fe oxide as a new type of presolar grain (Floss et al. 2008) is particularly noteworthy because this discovery would not have been made without the use of Auger spectroscopy for elemental characterization. We have used this technique also for the characterization of inclusions (Stadermann et al. 2006c) and pristine surfaces (Croat et al. 2009) of presolar SiC grains, as well as for the identification of individual presolar spinel grains from meteoritic residues (Gyngard et al. 2009). The exceptional surface sensitivity of this technique also aids in the analysis of cometary projectile residues in Al foil craters from the Stardust mission, even when the amounts of debris are too small for SEM-EDX measurements (Stadermann and Floss 2008b). This is especially important for the upcoming preliminary examination of interstellar material captured with the second Stardust collector (Westphal et al. 2008, 2009). We recently used Auger elemental imaging to detect thin layers of Fe-rich spray around hypervelocity impacts from space experiments in low earth orbit, an observation that may aid in obtaining trajectory information from such impacts (Stadermann et al. 2009).

We have determined elemental sensitivity factors for a set of ferromagnesian silicates and have found reproducibility in quantitative measurements within a few percent. It remains to be seen to what extent these sensitivity factors can also be used for other grain types. While this set of sensitivity factors

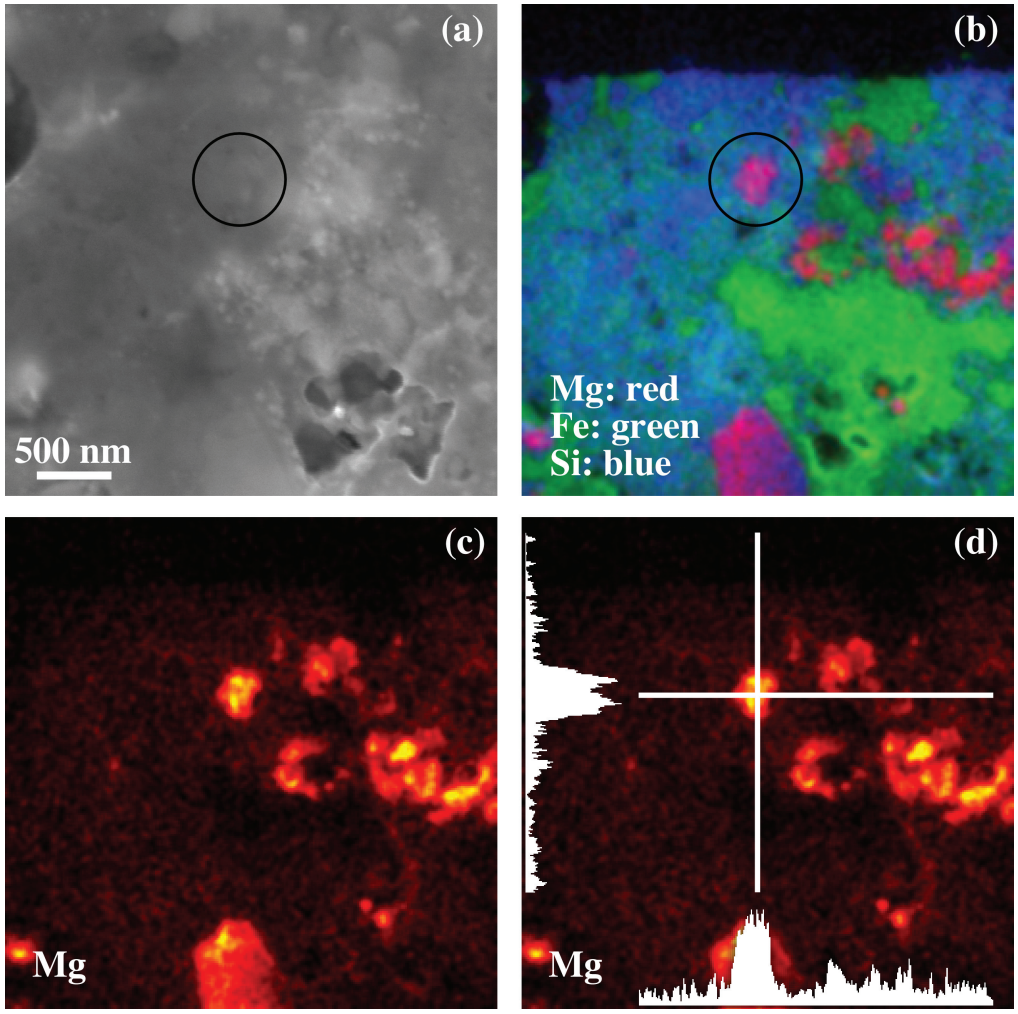

Fig. 11. Field-emission secondary electron (a) and Auger elemental images (b–d) of an area in the matrix of the CR chondrite MET 00426. NanoSIMS measurements indicate the presence of a presolar grain in the center of the circled area. Although no clear grain outlines are visible in the SE image (a), a distinct phase can be recognized in the Auger RGB false color image (b). The Mg-rich composition of this grain can also be seen in the Mg distribution map (c). Horizontal and vertical Mg line profiles (d) through the grain show relatively sharp edges of this phase, but also indicate a heterogeneous internal structure. The Auger spectrum of this grain "4c-3-o1" indicates a forsteritic olivine bulk composition (Floss and Stadermann 2009a). A subsequent FIB extraction and TEM study of this grain confirmed that it is distinctly enriched in Mg compared to the surrounding matrix, but also showed a compositional and structural heterogeneity on a ~10 nm scale (Stroud et al. 2009).

may also be applicable to amorphous grains with an overall ferromagnesian silicate composition, such samples are almost certainly more sensitive to electron beam damage and that by itself will result in less precise Auger quantifications. As mentioned above, we have found no significant discoloration (darkening) of the crystalline silicate standards under normal measurement conditions with a low beam current and a slightly rastered beam. However, such discolorations are occasionally observed under the same analytical conditions in the measurement of presolar silicate phases and it is possible that this difference is related to the crystallinity (or lack thereof) of the analyzed phase. Further studies will be required to investigate this relationship and whether it can be used for diagnostic purposes to distinguish crystalline and amorphous matter.

Auger electron energy spectra carry information not only about elemental abundances, but also details about the chemical states of elements in the analyzed sample. This "chemical fingerprinting" is well known in Auger spectroscopy and uses observations of the shapes and positions of the characteristic Auger peaks to obtain information about the bonding state of certain elements (Ramaker 2003). So far, we have not made explicit use of this technique, other than noting the fact that electron beam damage can lead to shifts in the position of the Si peaks. It remains to be seen to what extent the detailed study of Auger peaks can also be used as an additional tool for the identification of different mineral types that are relevant in cosmochemical studies. During the study of cometary residues in Al foil impact craters from the Stardust collector

(Stadermann et al. 2007) we have found that it is possible to distinguish, for example, between the Auger peaks of metallic Al from the foil and Al in individual mineral grains.

The key attribute of Auger spectroscopy is its ability to provide elemental information about the surface composition of a given sample on a spatial scale of less than 100 nm, without requiring special sample mounting or extraction. This capability makes Auger spectroscopy an ideal companion technique for the NanoSIMS by allowing correlated elemental and isotopic characterizations on a spatial scale that is relevant for the study of presolar grains in a variety of extraterrestrial host materials. The sample throughput, i.e., the number of analyzed samples per unit of analysis time, is comparable in both types of measurements and this fact greatly facilitates the side-by-side operation of both analytical techniques. Thus, Auger spectroscopy represents an important tool for the characterization of new types of presolar grains, as they are being located during NanoSIMS isotope imaging studies. Particularly interesting grains can then be selected on the basis of their isotopic and elemental composition for follow-up structural studies with the FIB-TEM technique and/or additional isotopic measurements. This is the approach that was used in the study of the presolar grain from Fig. 11, which was first analyzed in the NanoSIMS and the Auger spectrometer for its isotopic and elemental composition (Floss and Stadermann 2009a), followed by FIB extraction and TEM measurements for high resolution structural characterization (Stroud et al. 2009), before returning to the Auger spectrometer and the NanoSIMS for a second round of elemental and isotopic measurements directly in the FIB section. Such a complex and labor-intensive analytical path may not be practical for every presolar grain, but it demonstrates the value of combining different measurement types in the analysis of a single, sub-micrometer phase of interest.

Acknowledgments–A portion of the research described in this paper was performed in the Environmental Molecular Sciences Laboratory, a national scientific user facility sponsored by the Department of Energy's Office of Biological and Environmental Research and located at Pacific Northwest National Laboratory in Richland, Washington. Instrument purchase and development funding for the St. Louis work has been provided by NASA grants NNG06GE18G and NNX08AI13G (PI Stadermann). M. Bose is receiving support from NASA student fellowship NNX07AU80H. We are indebted to Dennis Paul and Physical Electronics of Chanhassen, Minnesota, for assistance and access to the Auger demonstration lab, as well as to Anne Hofmeister for graciously providing previously characterized silicate powder standards. We would also like to thank an anonymous reviewer for many detailed comments which helped improve the paper.

Editorial Handling—Dr. Gopalan Srinivasan

REFERENCES

Amari S., Lewis R. S., and Anders E. 1994. Interstellar grains in meteorites: I. Isolation of SiC, graphite, and diamond; size distributions of SiC and graphite. *Geochimica et Cosmochimica Acta* 58:459–470.

Auger P. 1975. The Auger effect. *Surface Science* 48:1–8.

Baer D. R., Gaspar D. J., Engelhard M. H., and Lea A. S. 2003. Beam effects during AES and XPS analysis. In *Surface analysis by Auger and X-ray photoelectron spectroscopy*, edited by Briggs D. and Grant J. T. IM Publications. pp. 211–233.

Bentley J., Gilliss S. R., Carter C. B., Al-Sharab J. F., Cosandey F., Anderson I. M., and Kotula P. J. 2006. Nanoscale EELS analysis of oxides: Composition mapping, valence determination and beam damage. *Journal of Physics* 26:69–72.

Bernatowicz T. and Walker R. M. 1997. Ancient stardust in the laboratory. *Physics Today* 50(12):26–32.

Bland P. A., Stadermann F. J., Floss C., Rost D., Vicenzi E. P., Kearsley A. T., and Benedix G. K. 2007. A cornucopia of presolar and early solar system materials at the micrometer size range in primitive chondrite matrix. *Meteoritics & Planetary Science* 42: 1417–1427.

Bose M., Floss C., and Stadermann F. J. 2007. Acfer 094 presolar silicates characterized using NanoSIMS and Auger nanoprobe (abstract). *Meteoritics & Planetary Science* 42:A23.

Bose M., Stadermann F. J., and Floss C. 2008a. An investigation into the origin of group 4 stardust grains (abstract #1099). 39th Lunar and Planetary Science Conference. CD-ROM.

Bose M., Floss C., and Stadermann F. J. 2008b. Iron-enriched stardust grains in the meteorites Acfer 094, QUE 99177, and MET 00426 (abstract). *Meteoritics & Planetary Science* 43:A27.

Childs K. D., Carlson B. A., Vanier L. A., Moulder J. F., Paul D. F., Stickle W. F., and Watson D. G. 1995. *Handbook of Auger electron spectroscopy*. Physical Electronics.

Croat T. K., Bernatowicz T., Amari S., Messenger S., and Stadermann F. J. 2003. Structural, chemical, and isotopic microanalytical investigations of graphite from supernovae. *Geochimica et Cosmochimica Acta* 67:4705–4725.

Croat T. K., Bernatowicz T. J., and Stadermann F. J. 2009. Auger and NanoSIMS investigations of pristine presolar SiC surfaces (abstract #1887). 40th Lunar and Planetary Science Conference. CD-ROM.

Croat T. K., Stadermann F. J., and Bernatowicz T. J. 2005. Presolar graphite from AGB stars: Microstructure and *s*-process enrichment. *The Astrophysical Journal* 631:976–987.

Daulton T. L., Bernatowicz T. J., Lewis R. S., Messenger S., Stadermann F. J., and Amari S. 2002. Polytype distribution in circumstellar silicon carbide. *Science* 296:1852–1855.

Daulton T. L., Bernatowicz T. J., Lewis R. S., Messenger S., Stadermann F. J., and Amari S. 2003. Polytype distribution of circumstellar silicon carbide: Microstructural characterization by transmission electron microscopy. *Geochimica et Cosmochimica Acta* 67:4743–4767.

Daulton T. L., Stadermann F. J., Bernatowicz T. J., Amari S., and Lewis R. S. 2006. First systematic TEM-NanoSIMS coordinated study of crystal structure and isotopic composition of presolar silicon carbide. *Meteoritics & Planetary Science* 41:A42.

Dikov Y. P., Wlotzka F., Ivanov A. V., Kantzel V. V., and Buleev M. I. 1999. Auger analysis of Apollo 17 orange soil sample 74220 (abstract #1176). 30th Lunar and Planetary Science Conference. CD-ROM.

Dran J. C., Duraud J. P., Klossa J., Langevin Y., and Maurette M. 1977. Microprobe studies of space weathering effects in extraterrestrial dust grains. *Philosophical Transactions of the Royal Society of London A* 285(1327):433–439.

Ecke G., Cimalla V., Tonisch K., Lebedev V., Romanus H., Ambacher O., and Liday J. 2007. Analysis of nanostructures by means of Auger electron spectroscopy. *Journal of Electrical Engineering* 58(6):301–306.

Floss C. and Stadermann F. J. 2007. Very high presolar grain abundances in the CR chondrite QUE 99177. *Meteoritics & Planetary Science* 42:A48.

Floss C. and Stadermann F. J. 2008a. The stardust inventories of CR chondrites QUE 99177 and MET 00426, and the distribution of presolar silicate and oxide grains in the early solar system (abstract #1280). 39th Lunar and Planetary Science Conference.

Floss C. and Stadermann F. J. 2008b. C-anomalous phases in QUE 99177 and MET 00426. *Meteoritics & Planetary Science* 43: A44.

Floss C. and Stadermann F. J. 2009a. Auger nanoprobe analysis of presolar ferromagnesian silicate grains from primitive CR chondrites QUE 99177 and MET 00426. *Geochimica et Cosmochimica Acta* 73:2415–2440.

Floss C. and Stadermann F. J. 2009b. High abundances of circumstellar and interstellar C-anomalous phases in the primitive CR3 chondrites QUE 99177 and MET 00426. *The Astrophysical Journal* 694:359–366.

Floss C., Stadermann F. J., and Bose M. 2008. Circumstellar Fe oxide from the Acfer 094 carbonaceous chondrite. *The Astrophysical Journal* 672:1266–1271.

Floss C., Stadermann F. J., Bradley J., Dai Z. R., Bajt S., and Graham G. 2004. Carbon and nitrogen isotopic anomalies in an anhydrous interplanetary dust particle. *Science* 303:1355–1358.

Floss C., Stadermann F. J., Nguyen A., Zinner E., and Lea A. S. 2005. High Fe contents in presolar silicate grains: Primary feature or the result of secondary processing? (abstract). *Meteoritics & Planetary Science* 40:A49.

Floss C., Stadermann F. J., Bradley J. P., Dai Z. R., Bajt S., Graham G., and Lea A. S. 2006. Identification of isotopically primitive interplanetary dust particles: A NanoSIMS isotopic imaging study. *Geochimica et Cosmochimica Acta* 70:2371–2399.

Floss C., Stadermann F. J., Mertz A., and Bernatowicz T. 2007. Anatomy of an isotopically primitive interplanetary dust particle: Coordinated NanoSIMS and Auger NanoProbe analyses (abstract #1145). 38th Lunar and Planetary Science Conference. CD-ROM.

Gold T., Bilson E., and Baron R. L. 1974. Observation of iron-rich coating on lunar grains and a relation to low albedo. 5th Lunar Science Conference. pp. 2413–2422.

Gold T., Bilson E., and Baron R. L. 1976. The surface composition of lunar samples and its significance for optical properties. 7th Lunar Science Conference. pp. 901–911.

Gold T., Bilson E., and Baron R. L. 1977. The relationship of surface chemistry and albedo of lunar soil samples. *Philosophical Transactions of the Royal Society of London A* 285(1327):427–431.

Goldstein J. I., Newbury D. E., Echlin P., Joy D. C., Romig A. D., Lyman C. E., Fiori C., and Lifshin E. 1992. *Scanning electron microscopy and X-ray microanalysis*. Plenum Press.

Graham G. A., Teslich N. E., Kearsley A. T., Stadermann F. J., Stroud R. M., Dai Z., Ishii H. A., Hutcheon I. A., Bajt S., Snead C. J., Weber P. K., and Bradley J. P. 2008. Applied focused ion beam techniques for sample preparation of astromaterials for integrated nanoanalysis. *Meteoritics & Planetary Science* 43:561–569.

Gyngard F., Morgand A., Nittler L. R., Stadermann F. J., and Zinner E. 2009. Extreme oxygen and magnesium isotopic anomalies in presolar spinel grains from the Murray carbonaceous meteorite (abstract #1386). 40th Lunar and Planetary Science Conference.

Henning T. 2009. Cosmic silicate dust. EAS Publication Series 35. pp. 103–114.

Hillion F., Daigne B., Girard F., and Slodzian G. 1993. A new high performance SIMS instrument: The Cameca "NanoSIMS 50." In *Secondary Ion Mass Spectrometry SIMS IX*, edited by A. Benninghoven, Y. Nihei, R. Shimizu, and H. W. Werner. Chichester: John Wiley & Sons. pp. 254–257.

Hillion F., Daigne B., Girard F., and Slodzian G. 1995. The CAMECA "NanoSIMS 50" experimental results. In *Secondary Ion Mass Spectrometry SIMS X* edited by A. Benninghoven, B. Hagenhoff, and H. W. Werner. Chichester: John Wiley & Sons. pp. 979–982.

Hochella M. F. Jr., Harris D. W., and Turner A. M. 1986a. Scanning Auger microscopy as a high-resolution microprobe for geologic materials. *American Mineralogist* 71:1247–1257.

Hochella M. F., Jr., Turner A. M., and Harris D. W. 1986b. High resolution scanning Auger microscopy of mineral surfaces. *Scanning Electron Microscopy* 337–349.

Hofmeister A. M. and Pitman K. M. 2007. Evidence for kinks in structural and thermodynamic properties across the forsterite-fayalite binary from thin-film IR absorption spectra. *Physics and Chemistry of Minerals* 34:319–333.

Huss G. R. 1997. The survival of presolar grains in solar system bodies. In *Astrophysical implications of the laboratory study of presolar materials,* edited by T. J. Bernatowicz and E. Zinner. American Institute of Physics. pp. 721–748.

Huss G. R. 2004. Implications of isotopic anomalies and presolar grains for the formation of the solar system. *Antarctic Meteorite Research* 17:132–152.

Kelly M. A. 2003. Analysing insulators with XPS and AES. In *Surface analysis by Auger and X-Ray photoelectron spectroscopy,* edited by Briggs D. and Grant J. T. IM Publications and SurfaceSpectra Ltd. pp. 191–210.

Kudo M. 2003. AES instrumentation and performance. In *Surface analysis by Auger and X-ray photoelectron spectroscopy,* edited by Briggs D. and Grant J. T. IM Publications. pp. 145–166.

Leitner J., Stephan T., Kearsley A. T., Hörz F., Flynn G. J., and Sandford S. A. 2008. TOF-SIMS analysis of crater residues from Wild 2 cometary particles on Stardust aluminum foil. *Meteoritics & Planetary Science* 43:161–185.

Lewis R. S., Tang M., Wacker J. F., Anders E., and Steel E. 1987. Interstellar diamonds in meteorites. *Nature* 326:160–162.

Mackinnon I. D. R. and Mogk D. W. 1985. Surface sulfur measurements on stratospheric particles. *Geophysical Research Letters* 12(2):93–96.

Marcus H. L. and Hackett L. H., Jr. 1974. The low temperature fracture behavior of iron-nickel meteorites. *Meteoritics* 9:371.

Marhas K. K., Hoppe P., Stadermann F. J., Floss C., and Lea A. S. 2006. The distribution of presolar grains in CI and CO meteorites (abstract #1959). 37th Lunar and Planetary Science Conference.CD-ROM.

Matrajt G., Ito M., Wirick S., Messenger S., Brownlee D. E., Joswiak D., Flynn G., Sandford S., Snead C., and A. W. 2008. Carbon investigation of two Stardust particles: A TEM, NanoSIMS, and XANES study. *Meteoritics & Planetary Science* 43:315–334.

McKeegan K. D., Aléon J., Bradley J., Brownlee D., Busemann H., Butterworth A., Chaussidon M., Fallon S., Floss C., Gilmour J., Gounelle M., Graham G., Guan Y., Heck P. R., Hoppe P., Hutcheon I. D., Huth J., Ishii H., Ito M., Jacobsen S. B., Kearsley A., Leshin L. A., Liu M.-C., Lyon I., Marhas K., Marty B., Matrajt G., Meibom A., Messenger S., Mostefaoui S., Mukhopadhyay S., Nakamura-Messenger K., Nittler L., Palma R., Pepin R. O., Papanastassiou D. A., Robert F., Schlutter D., Snead C. J., Stadermann F. J., Stroud R., Tsou P.,

Westphal A., Young E. D., Ziegler K., Zimmermann L., and Zinner E. 2006. Isotopic compositions of cometary matter returned by Stardust. *Science* 314:1724–1728.

Meeker G. P. 1986. Auger microprobe analysis of primitive solar system materials. *Meteoritics* 21:452–453.

Meeker G. P. and Fleming R. H. 1986. The use of microtomed thin sections for the analysis of geological materials with Auger electron spectrometry. *Microbeam Analysis* 1986:148–150.

Messenger S., Keller L. P., and Lauretta D. S. 2005. Supernova olivine from cometary dust. *Science* 309:737–741.

Messenger S., Keller L. P., Stadermann F. J., Walker R. M., and Zinner E. 2003. Samples of stars beyond the solar system: Silicate grains in interplanetary dust. *Science* 300:105–108.

Meyer B. S. and Zinner E. 2006. Nucleosynthesis. In *Meteorites and the early solar system II,* edited by Lauretta D. S. and McSween H. Y. Jr. Tucson: The University of Arizona. pp. 69–108.

Mogk D. W., Mackinnon I. D. R., and Rietmeijer F. J. M. 1985. Auger spectroscopy of stratospheric particles: The influence of aerosols on interplanetary dust (abstract). 16th Lunar and Planetary Science Conference. pp. 569–570.

Molster F. J. and Waters L. B. F. M. 2003. The mineralogy of interstellar and circumstellar dust. In *Astromineralogy*, edited by Henning T. Berlin: Springer-Verlag. pp. 121–170.

Mostefaoui S. and Hoppe P. 2004. Discovery of abundant in situ silicate and spinel grains from red giant stars in a primitive meteorite. *The Astrophysical Journal* 613:L149–L152.

Nagashima K., Krot A. N., and Yurimoto H. 2004. Stardust silicates from primitive meteorites. *Nature* 428:921–924.

Nakamura-Messenger K., Messenger S., Keller L. P., Clemett S. J., and Zolensky M. E. 2006. Organic globules in the Tagish Lake meteorite: Remnants of the protosolar disk. *Science* 314:1439–1442.

Nguyen A. N. and Zinner E. 2004. Discovery of ancient silicate stardust in a meteorite. *Science* 303:1496–1499.

Nguyen A. N., Stadermann F. J., Nittler L. R., and Alexander C. M. O'D. 2008. Characterization of presolar silicate and oxide grains using NanoSIMS and Auger spectroscopy (abstract #2142). 39th Lunar and Planetary Science Conference. CD-ROM.

Nguyen A. N., Stadermann F. J., Zinner E., Stroud R. M., Alexander C. M. O'D., and Nittler L. R. 2007. Characterization of presolar silicate and oxide grains in primitive carbonaceous chondrites. *The Astrophysical Journal* 656:1223–1240.

Nittler L. R., Alexander C. M. O'D., Gao X., Walker R. M., and Zinner E. 1997. Stellar sapphires: The properties and origins of presolar Al_2O_3 in meteorites. *The Astrophysical Journal* 483: 475–495.

Pantano C. G., D'Souza A. S., and Then A. M. 1998. Electron beam damage at solid surfaces. In *Beam effects, surface topography, and depth profiling in surface analysis*, vol. 5 edited by Czanderna A. W., Madey T. E., and Powell C. J. New York: Plenum Press. pp. 39–96.

Powell C. J. 2004. Effect of backscattered electrons on the analysis area in scanning Auger microscopy. *Applied Surface Science* 230:327–333.

Prutton M. and El Gomati M. M. 2006. *Scanning Auger electron microscopy.* Chichester: Wiley & Sons.

Radicati di Brozolo F., Ivanov I. C., and Anderson C. L. 1991. High resolution scanning Auger electron imaging of microtomed sections of Murchison matrix. 22nd Lunar and Planetary Science Conference. pp. 1107–1108.

Ramaker D. E. 2003. Chemical Information from Auger lineshapes. In *Surface analysis by Auger and X-ray Photoelectron Spectroscopy,* edited by Briggs D. and Grant J. T., pp. 465–500. IM Publications.

Savitzky A. and Golay M. 1964. Smoothing and differentiation of data by simplified least squares procedures. *Analytical Chemistry* 36:1627–1639.

Seah M. P. 2003a. Instrument calibration for AES and XPS. In *Surface analysis by Auger and X-ray photoelectron spectroscopy*, edited by Briggs D. and Grant J. T. IM Publications. pp. 167–189.

Seah M. P. 2003b. Quantification in AES and XPS. In *Surface analysis by Auger and X-ray photoelectron spectroscopy*, edited by Briggs D. and Grant J. T. IM Publications. pp. 345–375.

Seah M. P. and Spencer S. J. 2000. AES of bulk insulators—Control and characterisation of the surface charge. *Journals of Electron Spectroscopy and Related Phenomena* 109:291–308.

Seah M. P., Gilmore I. S., Bishop H. E., and Lorang G. 1998. Quantitative AES V. Practical analysis of intensities with detailed examples of metals and their oxides. *Surface and Interface Analysis* 26:701–722.

Slodzian G., Daigne B., Girard F., and Boust F. 1987. High sensitivity and high spatial resolution ion probe instrument. *SIMS VI.* pp. 189–192.

Smith G. C. 2005. Evaluation of a simple correction for the hydrocarbon contamination layer in quantitative surface analysis by XPS. *Journals of Electron Spectroscopy and Related Phenomena* 148:21–28.

Stadermann F. J., Croat T. K., Bernatowicz T. J., Amari S., Messenger S., Walker R. M., and Zinner E. 2005a. Supernova graphite in the NanoSIMS: Carbon, oxygen and titanium isotopic compositions of a spherule and its TiC sub-components. *Geochimica et Cosmochimica Acta* 69:177–188.

Stadermann F. J., Floss C., Bland P. A., Vicenzi E. P., and Rost D. 2005b. An oxygen-18 rich presolar silicate grain from the Acfer 094 meteorite: A NanoSIMS and TOF-SIMS study (abstract #2004). 36th Lunar and Planetary Science Conference. CD-ROM.

Stadermann F. J., Floss C., Zinner E., Nguyen A., and Lea A. S. 2005c. Auger spectroscopy as a complement to NanoSIMS studies of presolar materials (abstract). *Meteoritics & Planetary Science* 40:A146.

Stadermann F. J., Floss C., and Lea A. S. 2006a. Using Auger spectroscopy to characterize sub-micrometer presolar grains in situ: an overview (abstract #1663). 37th Lunar and Planetary Science Conference.

Stadermann F. J., Floss C., and Wopenka B. 2006b. Circumstellar aluminum oxide and silicon carbide in interplanetary dust particles. *Geochimica et Cosmochimica Acta* 70:6168–6179.

Stadermann F. J., Stephan T., Lea A. S., and Floss C. 2006c. The distribution of inclusions in a single large presolar silicon carbide grain (abstract). *Meteoritics & Planetary Science* 41:A166.

Stadermann F. J., Floss C., and Bose M. 2007. Correlated high spatial resolution elemental and isotopic characterization of Wild 2 cometary samples (abstract #1334). 38th Lunar and Planetary Science Conference. CD-ROM.

Stadermann F. J. and Floss C. 2008a. Abundance of presolar grains in comet Wild 2 and implications for transport and mixing in the solar nebula (abstract #1889). 39th Lunar and Planetary Science Conference. CD-ROM.

Stadermann F. J. and Floss C. 2008b. Determining the elemental and isotopic makeup of cosmic dust from residues in impact craters: preparation for the ISPE. *Meteoritics & Planetary Science* 43: A147.

Stadermann F. J., Hoppe P., Floss C., Heck P. R., Hörz F., Huth J., Kearsley A. T., Leitner J., Marhas K. K., McKeegan K. D., and Stephan T. 2008. Stardust in Stardust—The C, N, and O isotopic compositions of Wild 2 cometary matter in Al foil impacts. *Meteoritics & Planetary Science* 43:299–313.

Stadermann F. J., Floss C., Brownlee D. E., and Rodruck M. 2009. Revisiting LDEF: High resolution elemental and isotopic

characterization of hypervelocity impacts (abstract #2120). 40th Lunar and Planetary Science Conference. CD-ROM.

Stephan T. 2001. TOF-SIMS in cosmochemistry. *Planetary & Space Science* 49:859–906.

Stephan T., Leitner J., Floss C., and Stadermann F. J. 2003. TOF-SIMS analysis of isotopically anomalous phases in interplanetary dust and Renazzo (abstract #1343). 34th Lunar and Planetary Science Conference. CD-ROM.

Stroud R. M., Floss C., and Stadermann F. J. 2009. Structure, elemental composition and isotopic composition of presolar silicates in MET 00426 (abstract #1063). 40th Lunar and Planetary Science Conference. CD-ROM.

Stroud R. M., Nittler L. R., and Alexander C. M. O'D. 2004. Polymorphism in presolar Al_2O_3 grains from asymptotic giant branch stars. *Science* 305:1455–1457.

Tang M. and Anders E. 1988. Isotopic anomalies of Ne, Xe, and C in meteorites. II. Interstellar diamond and SiC: Carriers of exotic noble gases. *Geochimica et Cosmochimica Acta* 52:1235–1244.

Thompson M., Baker M. D., Christie A., and Tyson J. F. 1985. *Auger electron spectroscopy*. Chichester: Wiley & Sons.

Vollmer C., Stadermann F. J., Bose M., Floss C., Hoppe P., and Brenker F. E. 2007. Auger analysis of presolar silicates in Acfer 094 and the discovery of a presolar CAI (abstract). *Meteoritics & Planetary Science* 42:A158.

Vollmer C., Stadermann F. J., Floss C., Hoppe P., and Brenker F. E. 2008. Atypical magnesium abundances in oxygen-rich Stardust: NanoSIMS and Auger analyses (abstract). *Meteoritics & Planetary Science* 43:A164.

Vollmer C., Hoppe P., Stadermann F. J., Floss C., and Brenker F. E. 2009. NanoSIMS analysis and Auger electron spectroscopy of silicate and oxide stardust from the carbonaceous chondrite Acfer 094. *Geochimica et Cosmochimica Acta.*

Watts J. F. and Wolstenholme J. 2003. *An introduction to surface analysis by XPS and AES*. Chichester: Wiley & Sons.

Westphal A. J., Allen C., Bastien R., Borg J., Brenker F., Bridges J., Brownlee D. E., Butterworth A. L., Floss C., Flynn G., Frank D., Gainsforth Z., Grün E., Hoppe P., Kearsley A., Leroux H., Nittler L. R., Sandford S. A., Simionovici A., Stadermann F. J., Stroud R. M., Tsou P., Tyliczszak T., Warren J., and Zolensky M. E. 2008. Preliminary examination of the interstellar collector of Stardust (abstract #1855). 39th Lunar and Planetary Science Conference. CD-ROM.

Westphal A. J., Allen C., Bajt S., Basset R., Bastien R., Bechtel H., Bleuet P., Bor J., Brenker F. E., Bridges J. C., Brownlee D. E., Burchell M., Burghammer M., Butterworth A. L., Cloetens P., Cody G., Ferroir T., Floss C., Flynn G. J., Frank D., Gainsforth Z., Grun E., Hoppe P., Kearsley A., Lemelle L., Leroux H., Lettieri R., Marchant W., Mendez B., Nittler L. R., Ogliore R., Postberg F., Sandford S. A., Schmitz S., Silversmit G., Simionovici A., Srama R., Stadermann F. J., Stephan T., Stroud R. M., Susini J., Sutton S., Trielff M., Tsou P., Tsuchiyama A., Tyliczszak T., Vekemans B., Vincze L., Warren J. L., and Zolensky M. E. 2009. Stardust interstellar preliminary examination (ISPE) (abstract #1786). 40th Lunar and Planetary Science Conference. CD-ROM.

Yada T., Stadermann F. J., Floss C., Zinner E., Nakamura T., Noguchi T., and Lea A. S. 2006. High abundances of presolar silicates in Antarctic micrometeorites; implications for their cometary origins (abstract #1470). 37th Lunar and Planetary Science Conference. CD-ROM.

Yada T., Floss C., Stadermann F. J., Zinner E., Nakamura T., Noguchi T., and Lea S. 2008. Stardust in Antarctic micrometeorites. *Meteoritics & Planetary Science* 43:1287–1298.

Zalar A. 1985. Improved depth resolution by sample rotation during Auger electron spectroscopy depth profiling. *Thin Solid Films* 124:223–230.

Zega T. J., Nittler L., Busemann H., Hoppe P., and Stroud R. M. 2007. Coordinated isotopic and mineralogic analyses of planetary materials enabled by in situ lift-out with a focused ion beam scanning electron microscope. *Meteoritics & Planetary Science* 42:1373–1386.

Ziegler J. F., Biersack J. P., and Littmark U. 1985. *The stopping and range of ions in solids*. New York: Pergamon.

Zinner E. 1997. Presolar material in meteorites: An overview. In *Astrophysical implications of the laboratory study of presolar materials*, edited by T. J. Bernatowicz and E. Zinner. pp. 3–26. AIP.

Zinner E. 2007. Presolar grains. In *Treatise on geochemistry update*, vol. 1.02 (online update only), edited by H. D. Holland, K. K. Turekian, and A. Davis. Amsterdam: Elsevier. pp. 1–33.